Meta-Wall: Intelligent Omni-Surfaces Aided Multi-Cell MIMO Communications

Yutong Zhang[®], Graduate Student Member, IEEE, Boya Di[®], Member, IEEE, Hongliang Zhang[®], Member, IEEE, Zhu Han[®], Fellow, IEEE, H. Vincent Poor[®], Life Fellow, IEEE, and Lingyang Song[®], Fellow, IEEE

Abstract—Recently, reconfigurable intelligent surfaces (RISs) have been proposed as a novel solution to enhance wireless communications such as suppressing inter-cell interference. However, signals arriving at a conventional reflecting-type RIS can only be reflected towards one side, leading to a limited service coverage, especially in an indoor environment involving potential obstacles. In this paper, we consider an intelligent omni-surface (IOS) which can provide services for users on both sides by enabling simultaneous signal reflection and transmission. Specifically, we propose an IOS aided indoor communication system where an IOS is embedded in a wall between two independent access points (APs) to suppress inter-cell interference. Due to the independence of the APs, we design a distributed hybrid beamforming scheme consisting of digital beamforming at APs and IOS-based analog beamforming to maximize the sum rate without any exchange of channel state information (CSI) between APs. Simulation results indicate that the proposed system performs very close to an optimal centralized scheme, and has a better sum rate performance compared to existing schemes.

Index Terms—Intelligent omni-surface, reconfigurable intelligent surface, inter-cell interference, distributed hybrid beamforming.

I. INTRODUCTION

RIVEN by the explosive growth of the number of mobile devices, future wireless networks in beyond fifth generation (5G) and in sixth generation (6G) are required to provide high-speed and seamless data services for large numbers of users [1], [2]. However, mobile network performance is strongly limited by the complicated and dynamic wireless environment, especially for the indoor environment

Manuscript received 6 February 2021; revised 22 July 2021 and 15 November 2021; accepted 13 February 2022. Date of publication 8 March 2022; date of current version 12 September 2022. This work was supported in part by the National Key Research and Development Project of China under Grant 2020YFB1807100, in part by the Beijing Natural Science Foundation under Grant 4222005 and Grant L212027, and in part by the National Science Foundation under Grant 61931019 and Grant 61941101. The associate editor coordinating the review of this article and approving it for publication was A. Schmeink. (Corresponding authors: Lingyang Song; Boya Di.)

Yutong Zhang, Boya Di, and Lingyang Song are with the State Key Laboratory of Advanced Optical Communication Systems and Networks, School of Electronics, Peking University, Beijing 100871, China (e-mail: yutongzhang@pku.edu.cn; diboya@pku.edu.cn; lingyang.song@pku.edu.cn).

Hongliang Zhang and H. Vincent Poor are with the Department of Electrical and Computer Engineering, Princeton University, Princeton, NJ 08544 USA (e-mail: hongliang.zhang92@gmail.com; poor@princeton.edu).

Zhu Han is with the Electrical and Computer Engineering Department, University of Houston, Houston, TX 77004 USA, and also with the Department of Computer Science and Engineering, Kyung Hee University, Seoul 446-701, South Korea (e-mail: zhuhan22@gmail.com).

Color versions of one or more figures in this article are available at https://doi.org/10.1109/TWC.2022.3154041.

Digital Object Identifier 10.1109/TWC.2022.3154041

which involves random fading and potential obstacles (walls). In response to these issues, future indoor communication systems are expected to realize an intelligent and software reconfigurable paradigm [3], where parts of the indoor environment will adapt to time-varying wireless propagation, e.g., an *intelligent wall* [4]. Such an intelligent wall is capable of creating favorable propagation conditions, thereby providing much potential for a variety of future applications, such as wireless communication enhancement [5], sensing [6], localization [7], etc.

Fortunately, the recent development of metasurfaces provides a promising approach to make such an intelligent wall a reality by introducing new hardware technologies such as reconfigurable intelligent surfaces (RISs) [8]. Specifically, an RIS is an ultra-thin surface containing multiple subwavelength nearly-passive scattering elements with controllable electromagnetic properties, which enable the propagation environment to be reconfigurable [9]. Nevertheless, conventional reflecting-type RIS can only reflect signals towards one side of the surface, thereby restricting the service coverage [10], [11]. To provide network services to users on both sides of an intelligent wall, we consider a new instance of RIS, namely, the intelligent omni-surface (IOS) [12], which enables the signals that arrive at one side of the IOS to be simultaneously reflected and transmitted towards the users on both sides of the IOS [13].

In this paper, we propose an indoor communication system equipped with an IOS embedded intelligent wall. We consider the situation in which there are two adjacent rooms in each of which an access point (AP) is deployed to provide services to its subscribed users (SUs). Since the coverage of these two APs may overlap with each other, each SU can suffer from interference from the AP that it is not subscribed to. To mitigate this problem, we assume that an IOS is embedded in the wall between these two APs to create favorable propagation conditions. Due to their progammability, the IOS elements are capable of molding wavefronts into desired shapes, thereby realizing analog beamforming. In such an IOS aided system, the reflective/transmissive signals can be constructively added at the desired SUs to enhance the communication and destructively added at the unintended SUs to mitigate the interference simultaneously, thus significantly alleviate inter-cell interference.

Several previous studies have considered interference suppression with the assistance of one [14]–[17] or more [18]–[21] reflecting-type metasurfaces. For example, the

1536-1276 © 2022 IEEE. Personal use is permitted, but republication/redistribution requires IEEE permission. See https://www.ieee.org/publications/rights/index.html for more information.

authors in [14] studied a multigroup multicast system where a reflecting-type RIS was employed to enhance the power of the desired received signal and suppress the interference signal. The authors in [15] considered the analysis and optimization of quasi-static phase shift design in a reflectingtype RIS aided system in the presence of interference. The average rate and ergodic rate were maximized for both the instantaneous channel state information (CSI) case and the statistical CSI case. In [17], a reflecting-type RIS with joint transmission coordinated multipoint were combined to improve the data rate performance of the cell-edge users where the former was adopted to enhance the channel gain of cell-edge users and the latter was used to mitigate the inter-cell interference. In [18], a reflecting-type RIS was utilized to enhance the cell-edge performance in multi-cell MIMO communication systems. Active precoding at APs and the phase shifts at the RIS were jointly optimized to alleviate the inter-cell interference. A more general multi-RIS scenario was also investigated. The authors in [19] proposed a distributed design framework for cooperative beamforming to achieve inter-cell interference suppression with multiple reflecting-type RISs.

Most of the existing works employ conventional reflectingtype RISs to mitigate inter-cell interference where the data rate performance of SUs locating on the other side of the surface is not considered. Differently, in the proposed system, SUs on both sides of the surface can be served simultaneously by deploying an IOS embedded intelligent wall. Challenges arise in such a system. First, unlike the reflecting-type RIS aided systems [22], the power of the reflective and transmissive signals of the IOS may not be symmetric, leading to different channel models for the reflected and transmitted signals [23]. Therefore, the conventional reflecting-type RIS based beamforming schemes may not work any more and the optimal scheme is very challenging to obtain. Second, due to the independence of APs, it is difficult to exchange CSI between them, rendering a distributed mixed integer nonconvex optimization problem that is non-trivial to solve. Since the IOS embedded intelligent wall is shared between APs, the IOS based analog beamformer should be designed in a distributed manner to achieve a consensus between the two APs.

By addressing the above challenges, we contribute to state of the art in the following ways.

- We propose an IOS aided system where an IOS is embedded in the wall between two APs to suppress intercell interference. To maximize the sum rate, a hybrid beamforming scheme [24], [25] consisting of digital beamforming at APs and IOS-based analog beamforming is designed.
- 2) A sum rate maximization problem for the hybrid beamforming scheme is formulated. Considering the distributed nature of APs, we perform the hybrid beamforming scheme in a distributed manner, and proposed a distributed algorithm to mitigate inter-cell interference via IOS based analog beamforming design without any CSI exchange.

3) Simulation results indicate that the IOS aided system has a better sum rate performance compared to existing systems including the conventional cellular systems and two typical reflecting-type RIS aided systems, and performs very close to the optimal centralized scheme. The impact of the number of IOS elements, the number of quantization bits of discrete phase shifts, the ratio of transmissive SUs, the power ratio of transmissive signal to reflective signal, and the IOS location on sum rate are also shown numerically.

The rest of this paper is organized as follows. In Section II, we provide a system model of the IOS aided system with respect to the IOS model and the channel model. In Section III, the hybrid beamforming scheme is proposed for the IOS aided system, and a sum rate maximization problem is formulated. The hybrid beamforming design is performed in a distributed manner in Section IV to maximize the sum rate of all SUs. The convergence, complexity, and information exchange of the proposed scheme are also analyzed. The simulation results are given in Section V to evaluate the sum rate performance. Finally, we draw our conclusion in Section VI.

Notation: Scalars are denoted by Italic letters, vectors and matrices are denoted by bold-face lower-case and uppercase letters, respectively. \overline{a} denotes the complex conjugate of a complex scalar a. The real part and the imaginary part of a are denoted by $\text{Re}\{s\}$ and $\text{Im}\{s\}$, respectively. For a complex-valued vector \mathbf{x} , $\text{diag}(\mathbf{x})$ denotes a diagonal matrix each of whose diagonal element is the corresponding element in \mathbf{x} . For a square matrix \mathbf{S} , $\text{Tr}(\mathbf{S})$ denotes its trace. For any general matrix \mathbf{M} , \mathbf{M}^H denotes its conjugate transpose. I denotes an identity matrix.

II. SYSTEM MODEL

In this section, we first introduce a downlink indoor communication system where an IOS is embedded in the wall to alleviate inter-cell interference in Section II-A, and then present the IOS model and the channel model in Section II-B and II-C, respectively.

A. Scenario Description

As shown in Fig. 1, we consider a downlink transmission system in an indoor environment where the network services are provided by N=2 APs. For each AP n, the other AP is denoted as AP n'. Each AP is equipped with L antennas and subscribed by K single-antenna SUs, forming a virtual cell. Due to the coverage overlap of the two APs, each SU suffers severe interference from the AP which is not subscribed, especially for the SUs in the room of the non-subscribing AP, which are influenced by the blockage of the wall between adjacent rooms.

To tackle this problem, an IOS is embedded in the wall between the two APs as an autonomous part of a smart indoor environment to create favorable propagation conditions. Benefiting from the control on electromagnetic waves by the IOS, the signals arriving at the surface, i.e., desired signals

¹Such a narrowband system will be extended to a wideband case in our future work.

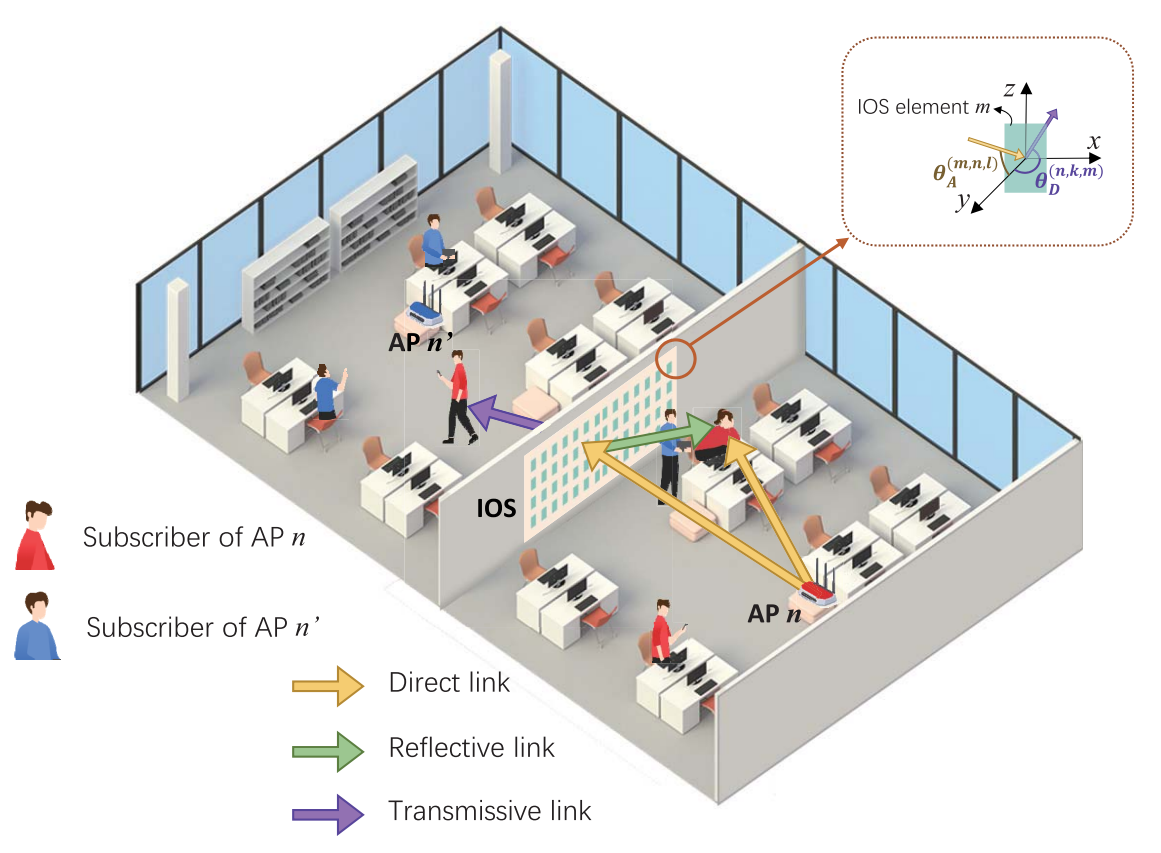


Fig. 1. IOS embedded intelligent wall for inter-cell interference suppression.

and interference, can be reflective and transmitted to the SUs simultaneously, and superimposed on the direct signals from APs.² Specifically, the reflective/transmissive signals can be constructively added at the desired SUs for communication enhancement or destructively added at the unintended SUs for interference suppression simultaneously. Therefore, the intercell interference can be significantly mitigated.

To achieve inter-cell interference suppression, two APs need to coordinate with each other, which requires extensive CSI exchange between APs. However, in practice, the two APs are independent with each other, making the information exchange difficult. Therefore, we consider a distributed hybrid beamforming scheme where only the location of APs and information about the IOS reflection and transmission coefficient design are exchanged via backhaul signaling. The details of the distributed hybrid beamforming scheme is presented in Section IV.

B. IOS Model

An IOS consists of M IOS elements each of which is a sub-wavelength meta-material particle with the size of $\delta_w \times \delta_h$. The electromagnetic responses of IOS elements can be manipulated towards incident waves via the ON/OFF operation of multiple connected electrically controllable PIN diodes. Benefit from these built-in programmable elements, IOS serves

²For the SUs which are in the room of the non-subscribing AP, the direct links between the AP and SUs are blocked by the wall. By deploying an IOS, these SUs can be served by the transmissive links.

as a reconfigurable phased array without extra active power sources which only relies on the combination of multiple IOS elements to realize a desired transformation on the received, reflective, or transmissive waves. When a signal arrives at an IOS element from either side of it, a part of the signal transmits through the elements as the *transmissive signal*, and a part of the signal is reflected as the *reflective signal* [29]. We consider the SUs served by transmissive and reflective signals as *transmissive SUs* and *reflective SUs*, respectively.

By a b-bit programmable meta-material, each IOS element can be configured into 2^b possible amplitudes/phase shifts to reflect or transmit the radio wave [30]. The phase shift ϕ_m of each IOS element m determines the waveform of the reflective and transmissive signals concurrently, and thus the reflection and transmission coefficient of the IOS element m [8] can be expressed by

$$q_{m} = \sqrt{G_{m} F_{A}^{(m,n,l)} F_{D}^{(n,k,m)} \delta_{h} \delta_{w} |\gamma_{m}|^{2}} e^{-j\phi_{m}},$$

$$\phi_{m} = \frac{i_{m} \pi}{2^{b-1}}, \quad i_{m} \in \{0, 1, \dots, 2^{b} - 1\},$$
(1)

where G_m is the antenna gain of IOS element m. γ_m is the power ratio of the departure signal, i.e., reflective or transmissive signal, to the arrival signal which is a function of the phase shift ϕ_m and can be obtained via experiments. $F_A^{(m,n,l)}$ and $F_D^{(n,k,m)}$ are the normalized power radiation patterns of the arrival signal and the departure signal, respectively, which

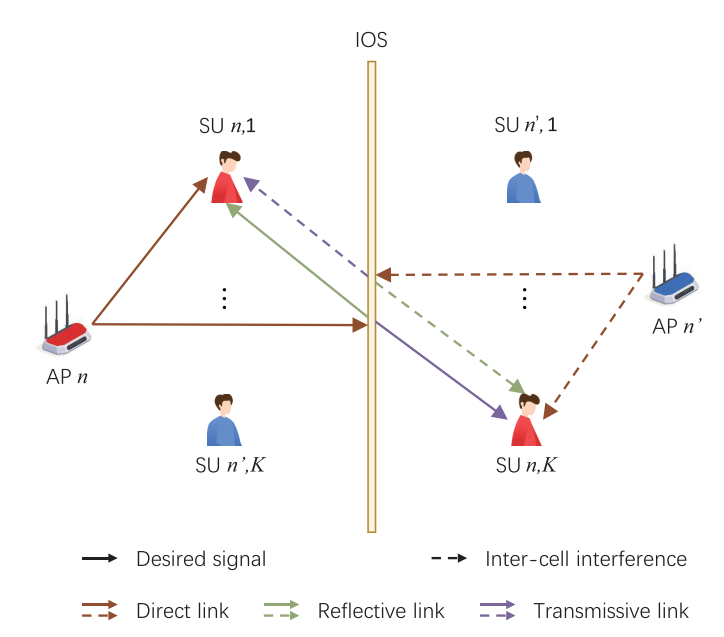


Fig. 2. Channel model for the IOS aided transmission system.

can be expressed by

$$F_A^{(m,n,l)} = |\cos^3 \theta_A^{(m,n,l)}|, \qquad (2)$$

$$F_D^{(n,k,m)} = \begin{cases} \frac{1}{1+\epsilon} |\cos^3 \theta_D^{(n,k,m)}|, & \theta_D^{(n,k,m)} \in (0, \frac{\pi}{2}), \\ \frac{\epsilon}{1+\epsilon} |\cos^3 (\pi - \theta_D^{(n,k,m)})|, & \theta_D^{(n,k,m)} \in (\frac{\pi}{2}, \pi). \end{cases}$$
(3)

As shown in Fig. 1, $\theta_A^{(m,n,l)}$ and $\theta_D^{(n,k,m)}$ are the angles between the arrival/departure signals and the *y*-axis. ϵ is a constant parameter indicating the power ratio of the transmissive signal to the reflective signal, which is determined by the structure and material of the IOS elements [31].

C. Channel Model

As shown in Fig. 2, the channel between each antenna of AP n and each SU (n,k), i.e., the k-th SU of AP n, consists of a direct link from AP n to SU (n,k) and M reflective-transmissive links via the IOS. To characterize the optimal performance of the IOS aided cellular system, we assume that the CSI of all channels is perfectly known at APs based on the various channel acquisition methods discussed in [26]–[28]. The channel models of the direct link and reflective-transmissive links are presented as follows.

1) Direct Link: We model the direct link $\mathbf{H}_D \in \mathbb{C}^{NK \times NL}$ between each AP to its SUs as a Rician channel, which can be given by

$$\mathbf{H}_D = \sqrt{\frac{\kappa}{1+\kappa}} \mathbf{H}_D^{LoS} + \sqrt{\frac{1}{1+\kappa}} \mathbf{H}_D^{NLoS}, \tag{4}$$

where κ is the Rician factor indicating the ratio of the line-of-sight (LoS) component to the non-line-of-sight (NLoS) one which are denoted by \mathbf{H}_D^{LoS} and \mathbf{H}_D^{NLoS} , respectively.

2) Reflective-Transmissive Link: To alleviate the intercell interference, an IOS is deployed to reflect and transmit arrived signals from APs and directly project to SUs. In this part, we model the reflective-transmissive link as a two-hop ray consisting of the channel between APs and IOS $\mathbf{H}_{AI} \in \mathbb{C}^{M \times NL}$ and that between IOS and SUs $\mathbf{H}_{IS} \in \mathbb{C}^{NK \times M}$, which can be formulated as the Rician models, expressed by

$$\mathbf{H}_{AI} = \sqrt{\frac{\kappa}{1+\kappa}} \mathbf{H}_{AI}^{LoS} + \sqrt{\frac{1}{1+\kappa}} \mathbf{H}_{AI}^{NLoS}, \tag{5}$$

$$\mathbf{H}_{IS} = \sqrt{\frac{\kappa}{1+\kappa}} \mathbf{H}_{IS}^{LoS} + \sqrt{\frac{1}{1+\kappa}} \mathbf{H}_{IS}^{NLoS}, \tag{6}$$

where \mathbf{H}_{AI}^{LoS} and \mathbf{H}_{IS}^{LoS} represent the LoS components of the AP-IOS link and the IOS-SU link, respectively, and \mathbf{H}_{AI}^{NLoS} and \mathbf{H}_{IS}^{NLoS} denote the NLoS ones.

The IOS reflects and transmits arrived signals based on an equivalent $M \times M$ diagonal reflective-transmissive coefficient matrix \mathbf{Q} consisting of the reflection and transmission coefficients $\{q_m\}$. Therefore, the equivalent channel $\mathbf{H} \in \mathbb{C}^{NK \times NL}$ can be given by³

$$\mathbf{H} = \underbrace{\mathbf{H}_{D}}_{\text{Direct link}} + \underbrace{\mathbf{H}_{IS}\mathbf{Q}\Gamma\mathbf{H}_{AI}}_{\text{Reflective-Transmissive link}}, \tag{7}$$

where Γ represents the spatial correlation matrix for the IOS elements. Specifically, the correlation coefficient between the m-th and the m'-th elements of the IOS can be given as [32]

$$\Gamma_{m,m'} = \operatorname{sinc}\left(\frac{2\|\mathbf{u}_m - \mathbf{u}_{m'}\|}{\lambda}\right),$$
 (8)

where λ is the wavelength and $\mathbf{u}_m = [0, \operatorname{mod}(m-1, \sqrt{M})\delta_h, \operatorname{mod}(m-1, \sqrt{M})\delta_w]^T$ denotes the location of m-th element of a $\sqrt{M} \times \sqrt{M}$ IOS.

Though we consider a downlink communication system in this paper, the results can be easily extended to an uplink case.

III. HYBRID BEAMFORMING AND PROBLEM FORMULATION

In this section, we first present a hybrid beamforming scheme based on the system model in Section III-A, and then formulate a sum rate maximization problem in Section III-B.

A. Hybrid Beamforming Scheme

Each IOS element can mold the wavefronts into desired shapes, inherently capable of realizing analog beamforming via determining the reflection and transmission coefficient of all IOS elements. Moreover, APs are responsible for the signal processing since IOS elements are passive devices without any digital processing capacity. To create reflective/transmissive waves towards preferable directions, we present a hybrid beamforming scheme for the proposed IOS aided system given the IOS model and the channel model. Specifically, the digital beamforming is performed at APs while the analog beamforming is achieved by the IOS.

³For the reflective SUs, the magnitude of the direct links is much larger than that of the reflective links. For the transmissive SUs, the channel gain of direct links is lower than that of the transmissive links since the former is blocked by obstructions.

1) Digital Beamforming: Each AP n encodes K different data streams for K SUs via a digital beamformer $\mathbf{V} \in \mathbb{C}^{NL \times NK}$, and then up-converts the encoded signals over the carrier frequency and allocates the transmit powers. We assume that $K \leq L$. The SUs' signals are sent directly through N APs each equipped with L antennas, which can be given by

$$x = Vs,$$
 (9

where $\mathbf{s} \in \mathbb{C}^{NK \times 1}$ denotes the incident signal vector for $N \times K$ SUs.

2) IOS-Based Analog Beamforming: In the IOS aided system, the analog beamforming is achieved by determining the reflection and transmission coefficient of all IOS elements, i.e., \mathbf{Q} , in a distributed manner. Specifically, the IOS with M elements performs a linear mapping from the incident signal vector to a reflective-transmissive signal vector. Therefore, the received signal at SU (n,k) can be expressed by (10), shown at the bottom of the page, where $\omega_{n,k} \sim \mathcal{CN}(0,\sigma^2)$ is the additive white Gaussian noise. $\mathbf{h}_D^{(n,k)}$ and $\mathbf{h}_{IS}^{(n,k)}$ denote the direct channel vector between all APs to SU (n,k) and the reflective-transmissive channel between the IOS and SU (n,k), i.e., the (n,k)-th row of matrices \mathbf{H}_D and \mathbf{H}_{IS} , respectively. $\mathbf{h}_{n,k}^n$ and $\mathbf{v}_{n,k}$ denote the channel vector between AP n and SU (n,k) and the digital beamforming vector used by AP n for transmitting data to SU (n,k).

B. Sum Rate Maximization Problem Formulation

Based on the IOS model, the channel model, and the hybrid beamforming scheme, the achievable data rate of SU (n,k) can be given by

$$R_{n,k} = \log_2 \left(1 + \frac{|\mathbf{h}_{n,k}^n \mathbf{v}_{n,k}|^2}{\sum_{k' \neq k} |\mathbf{h}_{n,k}^n \mathbf{v}_{n,k'}|^2 + \sum_{k'=1}^K |\mathbf{h}_{n,k}^{n'} \mathbf{v}_{n',k'}|^2 + \sigma^2} \right).$$
(11)

To study the effect of IOS on the SUs in terms of both reflective and transmissive signals, each AP aims to maximize the data rate of its SUs by jointly optimizing the digital beamforming \mathbf{V} and IOS based analog beamforming \mathbf{Q} . Consider \mathbf{Q} is determined by two APs distributedly, let \mathbf{Q}_n denotes the IOS based analog beamforming matrix determined by each AP n. The sum rate maximization problem can be formulated as

$$\max_{\mathbf{V},\mathbf{Q}} R = \sum_{n,k}^{N,K} R_{n,k}, \tag{12a}$$

s.t.
$$\operatorname{Tr}(\mathbf{V}_n^H \mathbf{V}_n) \le P_{max}^n$$
, (12b)

$$\mathbf{Q}_n = \mathbf{Q}_{n'},\tag{12c}$$

$$\mathbf{Q}_n \in \mathcal{F},$$
 (12d)

where $V_n = [\mathbf{v}_{n,1}, \mathbf{v}_{n,2}, \dots, \mathbf{v}_{n,K}]$ and \mathcal{F} is the feasible set of the IOS based analog beamformer according to (1). Constraint (12b) is the power constraints for APs, where P_{max}^n is the transmit power budget available at each AP n. Constraint (12c) is the consensus constraint to guarantee the IOS based analog beamforming matrix determined by each AP n, i.e., Q_n , is same as that determined by the other one. Constraint (12d) is the feasible set for the reflection and transmission coefficient of each IOS element.

Due to the distributed implementation of APs, the CSI cannot be shared between these APs, leading to a distributed mixed integer non-convex optimization problem which traditional algorithms, e.g., gradient search [33], are not applicable anymore. Therefore, in Section IV, we perform the hybrid beamforming scheme in a distributed manner, i.e., a distributed hybrid beamforming scheme, to mitigate the inter-cell interference via IOS based analog beamforming design without any CSI exchange. Specifically, AP n designs the IOS based analog beamforming egoistically to maximize the data rate of its SUs, and transmits the IOS based analog beamforming matrix to AP n'. After receiving the information from AP n, AP n' adjusts the IOS based analog beamforming according to the data rate performance of its SUs, and feeds it back to AP n, until a consensus is reached.

IV. DISTRIBUTED HYBRID BEAMFORMING DESIGN FOR SUM RATE MAXIMIZATION

To maximize the sum rate of the IOS based transmission system without extensive CSI exchange between APs, we propose a distributed hybrid beamforming scheme based on the alternating direction method of multipliers (ADMM) [34], [35]. Specifically, the digital beamformer of each AP is designed locally by itself and the IOS based analog beamforming matrix is determined by two APs in a distributed manner.

In the rest of this section, we first reformulate the sum rate maximization problem in (12) as the augmented Lagrangian function in Section IV-A, and then design the digital beamforming and the IOS based analog beamforming in Section IV-B and Section IV-C, respectively. Finally, we will summarize the overall algorithm and provide theoretical analysis of the proposed algorithm in SectionIV-D and Section IV-E, respectively.

A. Problem Reformulation

Due to the distributed implementation of APs, in this part, we first decouple problem (12) to enable two APs to maximize

$$z_{n,k} = (\mathbf{h}_D^{(n,k)} + \mathbf{h}_{IS}^{(n,k)} \mathbf{Q} \mathbf{\Gamma} \mathbf{H}_{AI}) \mathbf{v}_{n,k} \mathbf{s}_{n,k} + \omega_{n,k} = \underbrace{\mathbf{h}_{n,k}^n \mathbf{v}_{n,k} \mathbf{s}_{n,k}}_{\text{desired signals}} + \underbrace{\sum_{k' \neq k}^n \mathbf{h}_{n,k}^n \mathbf{v}_{n,k'} \mathbf{s}_{n,k'}}_{\text{intra-cell interference}} + \underbrace{\sum_{k'=1}^K \mathbf{h}_{n,k}^{n'} \mathbf{v}_{n',k'} \mathbf{s}_{n',k'}}_{\text{inter-cell interference}} + \omega_{n,k} \quad (10)$$

the sum rate in a distributed manner. Following that, the subproblem is reformulated as the augmented Lagrangian function based on the Lagrangian dual transform [36] and the fractional programming (FP) theory [37].

1) Lagrangian Dual Transform: To tackle the logarithm in (12), we now rewrite the sum-of-logarithms maximization problem in (12a) to a sum-of-ratios form by adopting the Lagrangian dual transform [36].

Lemma 1 (Lagrangian Dual Transform): Consider a sumof-logarithms maximization problem

$$\max_{u} \sum_{r=1}^{\mathcal{R}} \log_2 \left(1 + \frac{X_r(u)}{Y_r(u)} \right), \tag{13a}$$

$$s.t. \ u \in \mathcal{U}, \tag{13b}$$

where $X_r(u)$ and $Y_r(u)$ are nonnegative and positive functions, respectively, \mathcal{U} is a nonempty constraint set, the variable u can be discrete or continuous.

Problem (13) is equivalent to

$$\min_{u,\varrho} \sum_{r=1}^{\mathcal{R}} \left(\varrho_r - \log_2(1 + \varrho_r) - \frac{(1 + \varrho_r)X_r(u)}{X_r(u) + Y_r(u)} \right), \quad (14a)$$

 $s.t. \ u \in \mathcal{U}, \tag{14b}$

where ϱ_r is an auxiliary variable.

By adopting the Lagrangian dual transform, the subproblem solved by AP n is rewritten as

$$\min_{\mathbf{Q}_n, \mathbf{V}_n, \boldsymbol{\varrho}} f_1(\mathbf{Q}_n, \mathbf{V}_n, \boldsymbol{\varrho}), \tag{15a}$$

$$s.t. \operatorname{Tr}(\mathbf{V}_n^H \mathbf{V}_n) \le P_{max}^n, \tag{15b}$$

$$\mathbf{Q}_n = \mathbf{Q}_{n'},\tag{15c}$$

$$\mathbf{Q}_n \in \mathcal{F},\tag{15d}$$

where $f_1(\mathbf{Q}_n, \mathbf{V}_n, \boldsymbol{\varrho})$ can be expressed by (16), shown at the bottom of the page.

2) Fractional Programming Based Problem Reformulation: Note that problem (15) is the sum of the multiple-ratio FP problem, which can be rewritten by adopting the matrix quadratic transform [37], expressed by

$$\min_{\mathbf{Q}_n, \mathbf{V}_n \boldsymbol{\varrho}, \boldsymbol{\xi}} f_2(\mathbf{Q}_n, \mathbf{V}_n, \boldsymbol{\varrho}, \boldsymbol{\xi}), \tag{17a}$$

$$s.t. \operatorname{Tr}(\mathbf{V}_n^H \mathbf{V}_n) \le P_{max}^n, \tag{17b}$$

$$\mathbf{Q}_n = \mathbf{Q}_{n'},\tag{17c}$$

$$\mathbf{Q}_n \in \mathcal{F},\tag{17d}$$

where $\boldsymbol{\xi} = \{\xi_{n,k}\}$ is a collection of auxiliary variables. $f_2(\mathbf{Q}_n, \mathbf{V}_n, \boldsymbol{\varrho}, \boldsymbol{\xi})$ can be expressed by (18), shown at the bottom of the page.

3) The Augmented Lagrangian Function: To solve problem (17), we utilize the ADMM method, where the augmented Lagrangian function can be given by (19), shown at the bottom of the page, where μ_n is the dual variable introduced for the power constraint of each AP n. $\mathbb{I}(\cdot)$ is introduced to indicate whether the IOS based analog beamformer \mathbf{Q}_n is in the feasible set \mathcal{F} . Specifically, $\mathbb{I}(\mathbf{Q}_n) = 0$ if $\mathbf{Q}_n \in \mathcal{F}$, otherwise, $\mathbb{I}(\mathbf{Q}_n) = +\infty$. λ is the Lagrangian multiplier and $\rho > 0$. The optimal values of auxiliary variables $\boldsymbol{\varrho}$ and $\boldsymbol{\xi}$ can be calculated by the following Lemmas.

Lemma 2: The optimal $\varrho_{n,k}^*$ can be obtained by

$$\varrho_{n,k}^* = \frac{|\mathbf{h}_{n,k}^n \mathbf{v}_{n,k}|^2}{\sum_{k' \neq k} |\mathbf{h}_{n,k}^n \mathbf{v}_{n,k'}|^2 + \sum_{k'=1}^K |\mathbf{h}_{n,k}^{n'} \mathbf{v}_{n',k'}|^2 + \sigma^2}$$
(20)

Proof: Note that $f_1(\mathbf{Q}_n, \mathbf{V}_n, \varrho)$ is a concave differentiable function over ϱ with the fixed \mathbf{Q}_n and \mathbf{V}_n . Hence, the optimal $\varrho_{n,k}^*$ can be obtained by setting each $\frac{\partial f_1(\varrho_{n,k})}{\partial \varrho_{n,k}} = 0$.

Lemma 3: The optimal $\xi_{n,k}^*$ can be obtained by

$$\xi_{n,k}^* = \frac{\sqrt{1 + \varrho_{n,k}} \mathbf{h}_{n,k}^n \mathbf{v}_{n,k}}{\sum_{k'=1}^K |\mathbf{h}_{n,k}^n \mathbf{v}_{n,k'}|^2 + \sum_{k'=1}^K |\mathbf{h}_{n,k}^{n'} \mathbf{v}_{n',k'}|^2 + \sigma^2}$$
(21)

Proof: The optimal $\boldsymbol{\xi}^*$ can be obtained by minimizing each term in the summation in $f_2(\mathbf{Q}_n, \mathbf{V}_n, \boldsymbol{\xi})$ in (17) separately, expressed by

$$\xi_{n,k}^* = \arg\min_{\xi_{n,k}} f_2^{(n,k)},$$
 (22)

where

$$f_2^{(n,k)} = |\xi_{n,k}|^2 \Delta \xi_{n,k} - 2 \operatorname{Re} \{\xi_{n,k} \Lambda\} + \Upsilon$$

$$\stackrel{(a)}{=} (\xi_{n,k} - \Delta^{-1} \Lambda^H) \Delta (\xi_{n,k} - \Delta^{-1} \Lambda)$$

$$- \Lambda^H \Delta^{-1} \Lambda + \Upsilon. \tag{23}$$

$$f_{1}(\mathbf{Q}_{n}, \mathbf{V}_{n}, \boldsymbol{\varrho}) = \sum_{k=1}^{K} \left(\varrho_{n,k} - \log_{2}(1 + \varrho_{n,k}) - \frac{(1 + \varrho_{n,k})|\mathbf{h}_{n,k}^{n} \mathbf{v}_{n,k}|^{2}}{\sum_{k'=1}^{K} |\mathbf{h}_{n,k}^{n} \mathbf{v}_{n,k'}|^{2} + \sum_{k'=1}^{K} |\mathbf{h}_{n,k}^{n'} \mathbf{v}_{n',k'}|^{2} + \sigma^{2}} \right)$$
(16)

$$f_{2}(\mathbf{Q}_{n}, \mathbf{V}_{n}, \boldsymbol{\varrho}, \boldsymbol{\xi}) = \sum_{k=1}^{K} \left(|\xi_{n,k}|^{2} \sum_{k'=1}^{K} (|\mathbf{h}_{n,k}^{n} \mathbf{v}_{n,k'}|^{2} + |\mathbf{h}_{n,k}^{n'} \mathbf{v}_{n',k'}|^{2}) - 2\sqrt{1 + \varrho_{n,k}} \operatorname{Re}\{\xi_{n,k} \mathbf{h}_{n,k}^{n} \mathbf{v}_{n,k}\} + |\xi_{n,k}|^{2} \sigma^{2} + \varrho_{n,k} - \log_{2}(1 + \varrho_{n,k}) \right)$$
(18)

$$\mathcal{L}_n(\mathbf{Q}_n, \mathbf{V}_n, \boldsymbol{\lambda}_n) = f_2(\mathbf{Q}_n, \mathbf{V}_n, \boldsymbol{\varrho}, \boldsymbol{\xi}) + \mu_n [\text{Tr}(\mathbf{V}_n^H \mathbf{V}_n) - P_{max}^n] + \mathbb{I}(\mathbf{Q}_n) + \frac{\rho}{2} \|\mathbf{Q}_n - \mathbf{Q}_{n'} + \frac{\boldsymbol{\lambda}_n}{\rho}\|^2$$
(19)

(a) is obtained by completing the square [38]. The items in (23) which are independent of $\xi_{n,k}$ are denoted by

$$\Delta = \sum_{k'=1}^{K} (|\mathbf{h}_{n,k}^{n} \mathbf{v}_{n,k'}|^{2} + |\mathbf{h}_{n,k}^{n'} \mathbf{v}_{n',k'}|^{2}) + \sigma^{2}, \quad (24)$$

$$\Lambda = \sqrt{1 + \varrho_{n,k}} |\mathbf{h}_{n,k}^n \mathbf{v}_{n,k}|, \tag{25}$$

$$\Upsilon = \sigma_2 + \varrho_{n,k} - \log_2(1 + \varrho_{n,k}). \tag{26}$$

Hence, the optimal $\xi_{n,k}^*$ can be obtained by

$$\xi_{n,k}^* = \Delta^{-1} \Lambda = \frac{\sqrt{1 + \varrho_{n,k}} |\mathbf{h}_{n,k}^n \mathbf{v}_{n,k}|}{\sum_{k'=1}^K (|\mathbf{h}_{n,k}^n \mathbf{v}_{n,k'}|^2 + |\mathbf{h}_{n,k}^{n'} \mathbf{v}_{n',k'}|^2) + \sigma^2}.$$
(2

This completes the proof.

Based on the incremental ADMM, the digital beamforming matrix, the IOS based analog beamforming matrix, and the Lagrangian multiplier in the (t+1)-th iteration are updated as follows.

$$\mathbf{V}_n^{(t+1)} = \arg\min_{\mathbf{V}_n} \ \mathcal{L}_n(\mathbf{Q}_n^{(t)}, \mathbf{V}_n, \boldsymbol{\lambda}_n^{(t)}), \tag{28a}$$

$$\mathbf{Q}_n^{(t+1)} = \arg\min_{\mathbf{Q}_n} \ \mathcal{L}_n(\mathbf{Q}_n, \mathbf{V}_n^{(t+1)}, \boldsymbol{\lambda}_n^{(t)}),$$
 (28b)

$$\lambda_n^{(t+1)} = \lambda_n^{(t)} + \rho(\mathbf{Q}_n - \mathbf{Q}_{n'}). \tag{28c}$$

B. Digital Beamforming Design

To obtain the digital beamforming matrix V_n , the augmented Lagrangian function in (19) is rewritten as (29), shown at the bottom of the page, where $\bar{\xi}_{n,k}$ is the complex conjugate of $\xi_{n,k}$. C_1 is independent of $\mathbf{v}_{n,k}$, which can be given by (30), shown at the bottom of the page, where $\mathbf{V}_n^{(-k)}$ is obtained by setting the k-th column of \mathbf{V}_n as null. The minimum value of $\mathcal{L}_n(\mathbf{v}_{n,k})$ can be obtained with respect to $\mathbf{v}_{n,k}$ which satisfies

$$\frac{\partial \mathcal{L}_n(\mathbf{v}_{n,k})}{\partial \mathbf{v}_{n,k}} = 0. \tag{31}$$

The optimal value of $\mathbf{v}_{n,k}$ can be given by

$$\mathbf{v}_{n,k}^{*} = \frac{\sqrt{1 + \varrho_{n,k}} \operatorname{Re}\{\xi_{n,k}\} (\mathbf{h}_{n,k}^{n})^{H}}{\mu_{n} + \sum_{k'=1}^{K} |\xi_{n,k'}|^{2} (\mathbf{h}_{n,k}^{n})^{H} \mathbf{h}_{n,k}^{n}},$$
(32)

where μ_n is the normalized factor which is chosen to satisfy the power constraint in (12b).

Therefore, starting from a randomly initiated digital beamformer, the optimal V_n can be obtained by sequentially

updating each column for the SU (n,k), i.e., $\mathbf{v}_{n,k}$, in an iterative manner, until the algorithm converges to a local minimum of $\mathcal{L}_n(\mathbf{v}_{n,k})$.

C. IOS Based Analog Beamforming Design

To obtain the optimal IOS based analog beamforming matrix \mathbf{Q}_n , we rewrite the channel between AP n and SU (n,k) as

$$\mathbf{h}_{n,k}^{n} = \mathbf{h}_{D}^{(n,n,k)} + \mathbf{h}_{IS}^{(n,k)} \mathbf{Q}_{n} \mathbf{H}_{AI}^{(n)}$$

$$= \mathbf{h}_{D}^{(n,n,k)} + \tilde{\mathbf{q}}_{n} \tilde{\mathbf{H}}_{IS}^{(n,k)} \mathbf{H}_{AI}^{(n)}, \tag{33}$$

where $\tilde{\mathbf{q}}_n = [q_1^{(n)}, \dots, q_m^{(n)}]$ and $\tilde{\mathbf{H}}_{IS}^{(n,k)} = \operatorname{diag}(\mathbf{h}_{IS}^{(n,k)})$. Hence, the augmented Lagrangian function (19) is rewritten as

$$\mathcal{L}_n(\tilde{\mathbf{q}}_n) = \tilde{\mathbf{q}}_n \mathbf{A} \tilde{\mathbf{q}}_n^H + 2 \operatorname{Re} \{ \tilde{\mathbf{q}}_n \mathbf{B} \} + \mathbb{I}(\tilde{\mathbf{q}}_n) + \mathbf{C}_2, \quad (34)$$

where A, B, and C_2 are independent of \tilde{q}_n , which can be given by (35), shown at the bottom of the next page, (36), shown at the bottom of the next page, and (37), shown at the bottom of the next page, respectively.

Therefore, problem (17) can be reformulated as

$$\min_{\tilde{\mathbf{q}}_n} g(\tilde{\mathbf{q}}_n) = \tilde{\mathbf{q}}_n \mathbf{A} \tilde{\mathbf{q}}_n^H + 2 \operatorname{Re} \{ \tilde{\mathbf{q}}_n \mathbf{B} \},$$
 (38a)

$$s.t. \ \tilde{\mathbf{q}}_n \in \mathcal{F}. \tag{38b}$$

Although (38a) is a convex quadratic function, due to the non-convex constraint (38b), it is still hard to derive the optimal $\tilde{\mathbf{Q}}_n$. Therefore, problem (38) is further simplified based on the majorization-minimization (MM) strategy [39], [40] which consists of two steps. In the majorization step, given a point, a majorizer function is constructed which approximates the objective function, i.e., (38a), and satisfies that the minimum value of their difference is obtained at the current point. In the minimization step, we minimize the majorizer to obtain a near optimal solution.⁴

For the IOS based analog beamforming design, the majorizer of $g(\tilde{\mathbf{q}}_n)$ at point $\tilde{\mathbf{q}}_n^{(i)} \in \mathcal{F}$ can be given by (39), shown at the bottom of the next page, where Ω consists of elements $\{\sqrt{G_m\delta_h\delta_w|\gamma_m|^2}\}$ based on (1). ζ is the maximum eigenvalue of matrix \mathbf{A} . \mathbf{E} and \mathbf{F} are independent of $\tilde{\mathbf{q}}_n$, expressed by

$$\mathbf{E} = (\mathbf{A} - \zeta \mathbf{I})(\tilde{\mathbf{q}}_n^{(i)})^H + \mathbf{B},\tag{40}$$

$$\mathbf{F} = \zeta \mathbf{\Omega} \mathbf{\Omega}^H + \tilde{\mathbf{q}}_n^{(i)} (\zeta \mathbf{I} - \mathbf{A}) (\tilde{\mathbf{q}}_n^{(i)})^H. \tag{41}$$

⁴Numerical results proves that the suboptimal solution performs very close to the optimal approach, e.g., the exhaustive search method.

$$\mathcal{L}_{n}(\mathbf{v}_{n,k}) = -\sqrt{1 + \varrho_{n,k}} [\xi_{n,k} \mathbf{h}_{n,k}^{n} \mathbf{v}_{n,k} + \bar{\xi}_{n,k} \mathbf{v}_{n,k}^{H} (\mathbf{h}_{n,k}^{n})^{H}] + \mu_{n} \mathbf{v}_{n,k}^{H} \mathbf{v}_{n,k} + \sum_{k'=1}^{K} |\xi_{n,k'}|^{2} \cdot |\mathbf{h}_{n,k}^{n} \mathbf{v}_{n,k}|^{2} + \mathbf{C}_{1}$$
(29)

$$\mathbf{C}_{1} = \mu_{n} \operatorname{Tr}((\mathbf{V}_{n}^{(-k)})^{H} \mathbf{V}_{n}^{(-k)}) - \sum_{k' \neq k} \sqrt{1 + \varrho_{n,k'}} (\xi_{n,k'} \mathbf{h}_{n,k'}^{n} \mathbf{v}_{n,k'} + \bar{\xi}_{n,k'} \mathbf{v}_{n,k'}^{H} (\mathbf{h}_{n,k'}^{n})^{H})
+ \sum_{k=1}^{K} |\xi_{n,k}|^{2} (\sum_{k' \neq k} |\mathbf{h}_{n,k}^{n} \mathbf{v}_{n,k'}|^{2} + \sum_{k'=1}^{K} |\mathbf{h}_{n,k}^{n'} \mathbf{v}_{n',k'}|^{2}) + \mathbb{I}(\mathbf{Q}_{n}) + \frac{\rho}{2} ||\mathbf{Q}_{n} - \mathbf{Q}_{n'} + \frac{\lambda_{n}}{\rho}||^{2}$$
(30)

Therefore, the closed-from solution of problem (38) can be obtained by minimizing $\text{Re}\{\tilde{\mathbf{q}}_n\mathbf{E}\}$, which can be calculated by

$$\tilde{\mathbf{q}}_n^* = -\mathbf{\Omega} \circ (e^{-j\angle \mathbf{E}}),\tag{42}$$

where $\angle \mathbf{E}$ denotes the argument of \mathbf{E} .

D. Overall Algorithm Description

In this section, we propose a distributed hybrid beamforming scheme to solve the sum rate maximization problem (12) without any CSI exchange. For initialization, these two APs share their locations and set the random digital beamforming and IOS based analog beamforming matrices. At the (t+1)-th iteration, each AP n updates the digital beamforming matrix $\mathbf{V}_n^{(t+1)}$, the IOS based analog beamforming matrix $\tilde{\mathbf{q}}_n^{(t+1)}$, and the Lagrangian multiplier $\lambda_n^{(t+1)}$ are incrementally updated according to (32), (42), and (28c), respectively. After that, $\mathbf{V}_n^{(t+1)}$ and $\tilde{\mathbf{q}}_n^{(t+1)}$ are transmitted from AP n to AP n'. The discrete beamforming design algorithm is summarized in Algorithm 1.

E. Properties of the Distributed Hybrid Beamforming Design

We now analyze the convergence, computational complexity, and information exchange of the distributed hybrid beamforming scheme.

1) Convergence: To guarantee the IOS based analog beamforming matrices determined by two APs converge to the same value, the consensus constraint (17c) is introduced and acts as a penalty term $\frac{\rho}{2} \|\mathbf{Q}_n - \mathbf{Q}_{n'} + \frac{\lambda_n}{\rho}\|^2$ in (19). By performing Step 7 of Algorithm 1, for each AP n, the penalty term is optimized to a minimal value with the fixed λ_n . Hence, a smaller gap between \mathbf{Q}_n and $\mathbf{Q}_{n'}$, i.e., $\triangle \mathbf{Q}$, can be achieved

```
Algorithm 1 Distributed Hybrid Beamforming Design Algorithm
```

Input: Channel matrices \mathbf{H}_D , \mathbf{H}_{AI} , \mathbf{H}_{LS}

```
Output: The digital beamformer V, the IOS based analog beamformer Q

1 Initialize V, Q, \lambda;
2 for each iteration t+1 do

3 | for each AP n do

4 | Obtain the optimal \varrho^* according to (20);
Obtain the optimal \xi^* according to (21);
Update \mu_n^{(t+1)} and \mathbf{V}_n^{(t+1)} according to (32);
Update \mathbf{Q}_n^{(t+1)} according to (42);
Update \lambda_n^{(t+1)} according to (28c);
Transmit \mathbf{V}_n^{(t+1)}, \mathbf{Q}_n^{(t+1)} to AP n';
10 | end
```

in each iteration, expressed by

$$\triangle \mathbf{Q}^{(t+1)} \leqslant \triangle \mathbf{Q}^{(t)}. \tag{43}$$

This indicates that the IOS based analog beamforming matrix determined by each AP n approaches to that determined by the other one after each iteration, and thus the proposed algorithm is guaranteed to converge.

- 2) Computational Complexity: Note that the complexity mainly depends on the digital beamforming design and the IOS based analog beamforming design. We now analyze the computational complexity of each iteration of Algorithm 1 for these two parts separately.
 - Digital beamforming: Each $\mathbf{v}_{n,k}$ is updated sequentially to obtain the optimal \mathbf{V}_n according to the closed-form expression in (32). Therefore, the complexity of digital

$$\mathbf{A} = \frac{\rho}{2}\mathbf{I} + \sum_{k=1}^{K} |\xi_{n,k}|^{2} \sum_{k'=1}^{K} (\tilde{\mathbf{H}}_{IS}^{(n,k)} \mathbf{H}_{AI}^{(n)} \mathbf{v}_{n,k'} \mathbf{v}_{n,k'}^{H} (\mathbf{H}_{AI}^{(n)})^{H} (\tilde{\mathbf{H}}_{IS}^{(n,k)})^{H} + \tilde{\mathbf{H}}_{IS}^{(n',k)} \mathbf{H}_{AI}^{(n')} \mathbf{v}_{n',k'} \mathbf{v}_{n',k'}^{H} (\mathbf{H}_{AI}^{(n')})^{H} (\tilde{\mathbf{H}}_{IS}^{(n',k)})^{H})$$
(35)
$$\mathbf{B} = \frac{\lambda_{n}^{H}}{2} - \frac{\rho}{2} \tilde{\mathbf{q}}_{n'} + \sum_{k=1}^{K} (|\xi_{n,k}|^{2} \sum_{k'=1}^{K} (\tilde{\mathbf{H}}_{IS}^{(n,k)} \mathbf{H}_{AI}^{(n)} \mathbf{v}_{n,k'} \mathbf{v}_{n,k'}^{H} (\mathbf{h}_{D}^{(n,n,k)})^{H} + \tilde{\mathbf{H}}_{IS}^{(n',k)} \mathbf{H}_{AI}^{(n)} \mathbf{v}_{n,k})^{H} + \tilde{\mathbf{H}}_{IS}^{(n',k)} \mathbf{H}_{AI}^{(n',k)} \mathbf{v}_{n,k})$$
(36)
$$\mathbf{C}_{2} = |\xi_{n,k}|^{2} \sum_{k=1}^{K} \sum_{k'=1}^{K} \left(\mathbf{h}_{D}^{(n,n,k)} \mathbf{v}_{n,k'} \mathbf{v}_{n,k'}^{H} (\mathbf{h}_{D}^{(n,n,k)})^{H} + \mathbf{h}_{D}^{(n',n,k)} \mathbf{v}_{n',k'} \mathbf{v}_{n',k'}^{H} (\mathbf{h}_{D}^{(n',n,k)})^{H} \right)$$

$$-2 \sum_{k=1}^{K} \sqrt{1 + \varrho_{n,k}} \operatorname{Re} \{ \xi_{n,k} \mathbf{h}_{D}^{(n,n,k)} \mathbf{v}_{n,k} \} + \sum_{k=1}^{K} \left(|\xi_{n,k}|^{2} \sigma^{2} + \varrho_{n,k} - \log_{2}(1 + \varrho_{n,k}) \right)$$

$$+ \mu_{n} [\operatorname{Tr}(\mathbf{V}_{n}^{H} \mathbf{V}_{n}) - P_{max}^{n}] + \tilde{\mathbf{q}}_{n'} \tilde{\mathbf{q}}_{n'}^{H} - \tilde{\mathbf{q}}_{n'} + \frac{\lambda_{n}}{\rho} - \frac{\lambda_{n}}{\rho} \tilde{\mathbf{q}}_{n'}^{H} + \frac{\lambda_{n} \lambda_{n}^{H}}{\rho^{2}}$$
 (37)

$$g(\tilde{\mathbf{q}}_{n}, \tilde{\mathbf{q}}_{n}^{(i)}) = \zeta \tilde{\mathbf{q}}_{n} \tilde{\mathbf{q}}_{n}^{H} + 2 \operatorname{Re} \{ \tilde{\mathbf{q}}_{n} (\mathbf{A} - \zeta \mathbf{I}) (\tilde{\mathbf{q}}_{n}^{(i)})^{H} \} + \tilde{\mathbf{q}}_{n}^{(i)} (\zeta \mathbf{I} - \mathbf{A}) (\tilde{\mathbf{q}}_{n}^{(i)})^{H} + 2 \operatorname{Re} \{ \tilde{\mathbf{q}}_{n} \mathbf{B} \}$$

$$= \zeta \Omega \Omega^{H} + 2 \operatorname{Re} \{ \tilde{\mathbf{q}}_{n} [(\mathbf{A} - \zeta \mathbf{I}) (\tilde{\mathbf{q}}_{n}^{(i)})^{H} + \mathbf{B}] \} + \tilde{\mathbf{q}}_{n}^{(i)} (\zeta \mathbf{I} - \mathbf{A}) (\tilde{\mathbf{q}}_{n}^{(i)})^{H}$$

$$= 2 \operatorname{Re} \{ \tilde{\mathbf{q}}_{n} \mathbf{E} \} + \mathbf{F}$$
(39)

beamforming design is $\mathcal{O}(I_dK)$, where I_d is the number of iterations used for digital beamforming design.

• IOS based analog beamforming: \mathbf{Q} is optimized by adopting the MM method which leads to the complexity of $\mathcal{O}(I_iM^3)$, where I_i is the number of iterations used for IOS based analog beamforming design.

Therefore, the complexity of Algorithm 1 is $\mathcal{O}(2I_dK + 2I_iM^3)$ in each iteration.

3) Information Exchange: Due to the distributed implementation, it is difficult to exchange and share information between these two APs. By adopting Algorithm 1, only three variables are incrementally updated and transmitted to the other AP, i.e., the digital beamforming matrix \mathbf{V}_n , the IOS based analog beamforming matrix $\tilde{\mathbf{q}}_n$, and the location of each AP, where the last one only has to be exchanged once. The amount of total required backhaul signaling of the proposed algorithm is 2+2I(KL+M), where I is the number of iterations used for adopting Algorithm 1.

V. SIMULATION RESULTS

In this section, we evaluate our proposed distributed hybrid beamforming for the IOS aided transmission system in terms of the sum rate. We show how the sum rate is influenced by the transmit power per AP, the number of IOS elements, the number of quantization bits for discrete phase shifts, the location of the IOS, the ratio of transmissive SUs to all SUs, and the power ratio of transmissive signal to reflective signal ϵ . For comparison, the following schemes are considered as benchmarks.

- 1) Centralized scheme: We consider the centralized scheme as an upper bound to evaluate the sum rate performance of the distributed hybrid beamforming scheme where the hybrid beamforming is designed by a center controller using the algorithm in [20].
- Conventional cellular system: Conventional cellular networks without IOS. SUs in the cellular system receive signals only via direct links from APs without the assistance of the IOS.
- 3) Reflecting-type RIS aided system (middle): A reflecting-type RIS is embedded in the wall between two rooms, and the signals arriving at the surface cannot be transmitted to the other side.
- 4) Reflecting-type RIS aided system (side): A reflecting-type RIS is embedded in the outer wall of one of these two rooms, i.e., all APs and SUs are on the same side of the surface. Therefore, all SUs can be served by both direct links and reflection links.

For the propagations, we use the InH path loss model certified by the International Telecommunication Union (ITU) [41] which is usually applied in the indoor environment as the distance-dependent channel path loss model. Specifically, the direct channel between AP n and its SUs in room n' is set as

$$PL_{obs} = 43\log_{10}(d) + 11.5 + 20\log_{10}(f_c),$$
 (44)

which is a typical model of the obstructed-in-building case. d and f_c denote the distance between AP n and its SUs in room n' and the carry frequency. In contrast, other channels

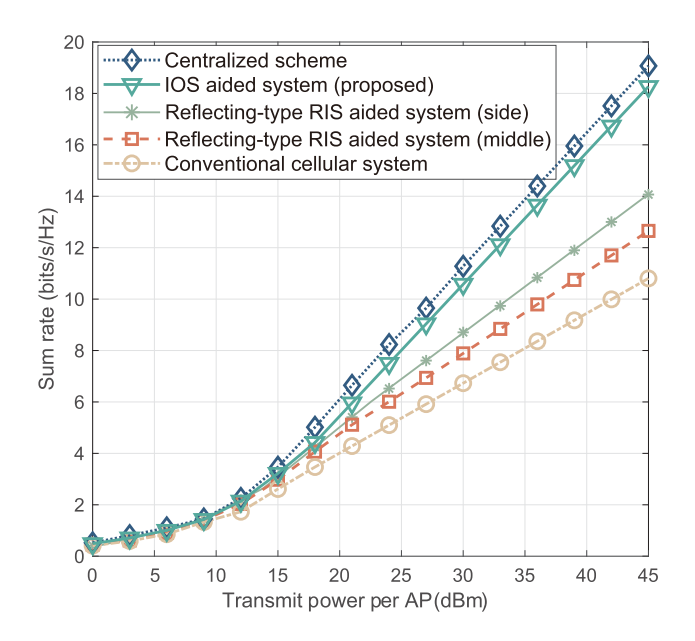


Fig. 3. Sum rate vs. transmit power per AP of different schemes.

without obstacles are modeled as

$$PL_{Nobs} = 16.9 \log_{10}(d) + 32.8 + 20 \log_{10}(f_c).$$
 (45)

For simulation, we consider the Rician fading channel model for all channels. Without loss of generality [5]–[8], the spatial correlation matrix are set to identity matrix for simplicity. Simulation parameters are set up based on the existing works [13], [25], as given in TABLE I.

A. Comparison With Benchmarks

Fig. 3 shows the sum rate of the IOS aided transmission system versus the transmit power per AP P_{max} , obtained by different schemes with 100 IOS elements, i.e., M=100. The number of quantization bits for discrete phase shifts b is set as 3. We set half of SUs as transmissive SUs. The distance between SUs and the IOS and the power ratio of transmissive signal to reflective signal ϵ are set as 5m and 1, respectively.

We observe that the sum rate of different schemes grows with the transmit power per AP. The IOS aided system achieves a better sum rate performance than the conventional cellular system and two reflecting-type RIS aided systems, and performs very close to the centralized scheme. Compared with the conventional cellular system, we observe that the IOS deployed in the building can effectively improve the sum rate performance of the cellular communication system. Compared with the reflecting-type RIS aided system (middle), it can be seen that the IOS aided system achieves a better sum rate performance since SUs on both sides can be served by the reflective-transmissive links, implying that the spatial resources are better utilized. In the reflecting-type RIS aided system (side), all APs and SUs are on the same side of the surface, and thus, the SUs in the room of non-subscribing AP can be served by signal reflection, thereby achieving a higher sum rate than the reflecting-type RIS aided system (middle). However, the reflective links of SUs in the room without the reflecting-type RIS are still influenced by the wall between

TABLE I SIMULATION PARAMETERS

Parameter	Value
Rician factor κ	4
Number of antennas of each AP L	8
Number of SUs K	8
Noise power σ^2	-96 dBm
Carrier frequency f_c	5.9GHz
Bandwidth	20MHz
Width of each IOS element δ_w	0.02m
Height of each IOS element δ_h	0.02m
Inter-distance between adjacent IOS elements	0.025m
Antenna gain of IOS element m G_m	1
Power ratio of the departure signal to the arrival signal γ_m	1
The height of APs and the center of the IOS	2m
Size of each room	50m×50m
The thickness of the wall	0.05m

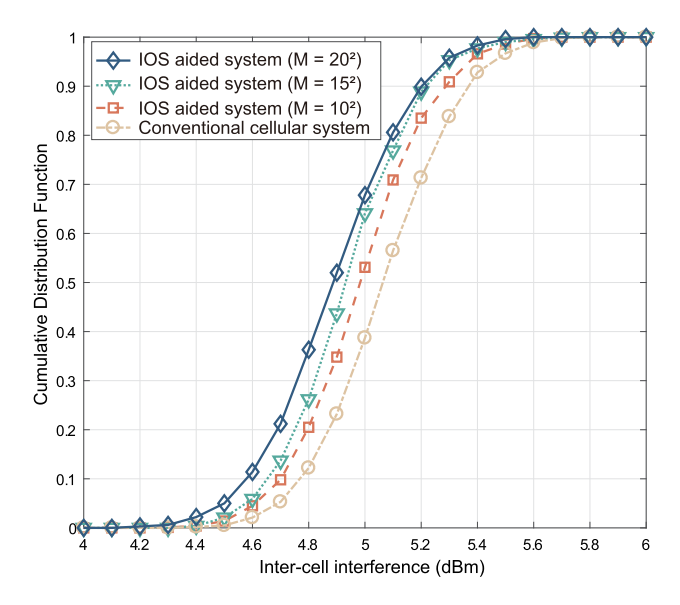


Fig. 4. C.D.F. of the inter-cell interference of different schemes.

these two rooms. Therefore, the proposed IOS aided system can obtain a better sum rate performance.

B. Inter-Cell Interference Suppression

Fig. 4 shows the cumulative distribution function (C.D.F.) of the inter-cell interference of the IOS aided system and traditional cellular system without IOS, respectively. The transmit power per AP P_{max} is set as 43 dBm. The IOS consists of M=100 elements each of which works with b=3 quantization bits for discrete phase shifts. The ratio of transmissive SUs to all SUs is set as 0.5. The distance between SUs and the IOS and the power ratio of transmissive signal to reflective signal ϵ are set as 5m and 1, respectively. We observe that, compare to the cellular system, the IOS aided system obtains a higher value of C.D.F. of the intercell interference and converges to 1 faster. It implies that the

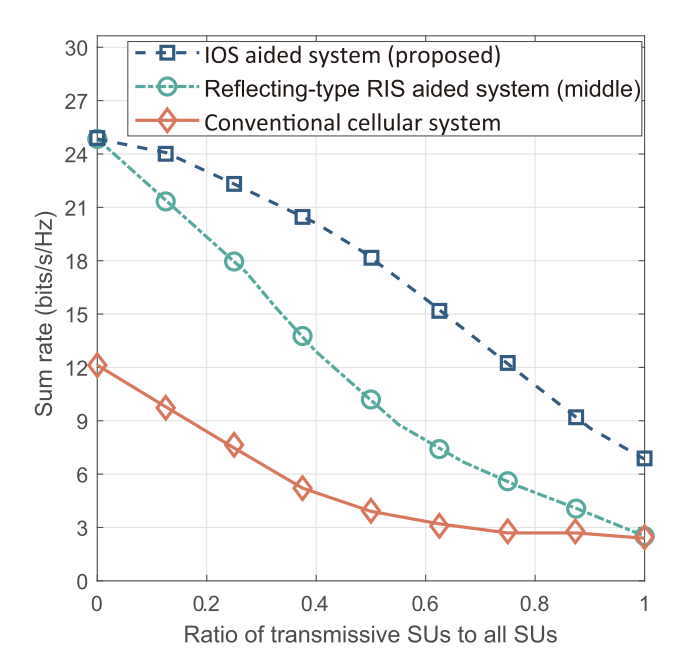


Fig. 5. Sum rate vs. the ratio of transmissive SUs to all SUs.

inter-cell interference can be alleviated efficiently by deploying the IOS since the interference signals through the IOS can be destructively transmit to directions without SUs. As the number of IOS elements increases, more signals from AP n to the other room are transmitted through the IOS rather than the wall, leading to a lower inter-cell interference.

C. Impact of Ratio of Transmissive SUs

Fig. 5 depicts the sum rate versus the ratio of transmissive SUs to all SUs with different schemes. There are M=100 IOS elements and each of them works with b=3 quantization bits for discrete phase shifts. The distance between SUs and the IOS and the power ratio of transmissive signal to reflective signal ϵ are set as 5m and 1, respectively. The transmit power per AP P_{max} is set as 43 dBm.

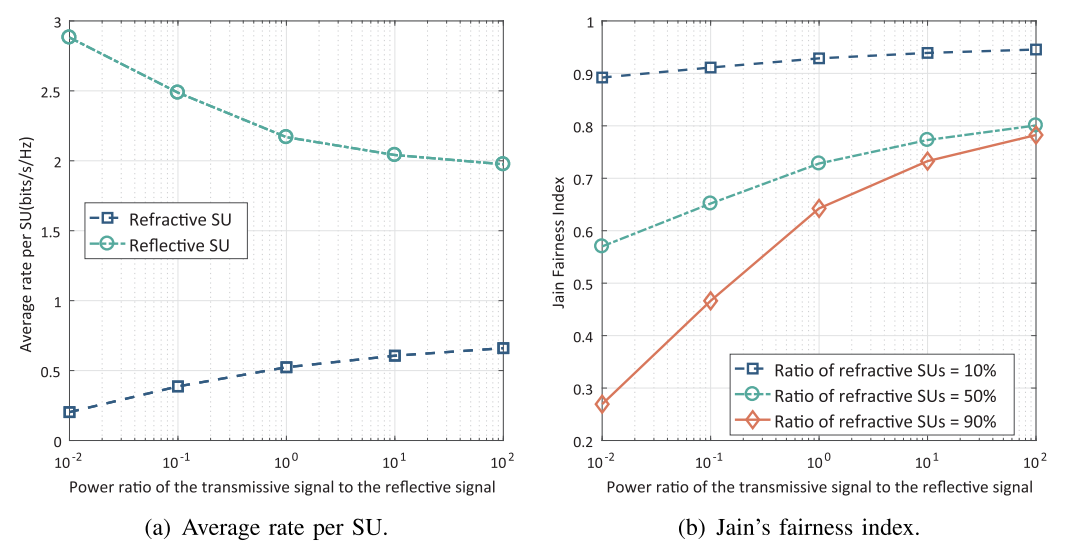


Fig. 6. The impact of the power ratio of transmissive signal to reflective signal ϵ .

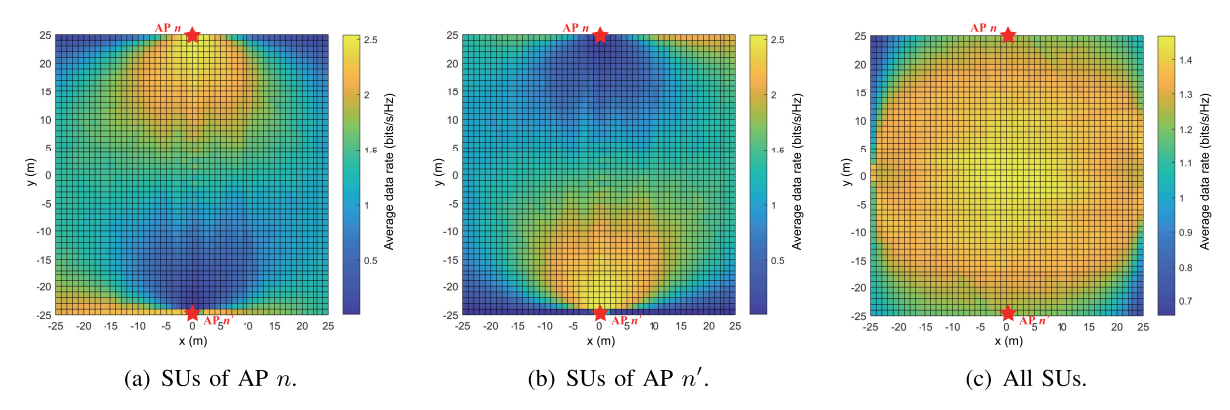


Fig. 7. The impact of IOS location on the average data rate performance (The value of each point illustrates the average data rate when the center of the IOS is located at (x, y)).

Since the wall blocks the direct signal from AP n to its SUs in room n', the available rate of transmissive SUs is lower than that of reflective SUs. Therefore, as the ratio of transmissive SUs to all SUs grows, the sum rate decreases by adopting different schemes. Compared with the conventional cellular system and the reflecting-type RIS aided system (middle), a better sum rate performance is achieved by the proposed scheme since signals can be transmitted through the IOS to enhance the communication for transmissive SUs. When all SUs are in the same room with their subscribing APs, i.e., the ratio of transmissive SUs to all SUs is 0, the IOS only works in a reflection mode which is equal to the reflectingtype RIS aided system (middle). Moreover, when the ratio of transmissive SUs to all SUs is 1, the reflecting-type RIS aided system (middle) provides services for SUs only via direct links, thereby obtaining the same sum rate with the conventional cellular system.

D. Impact of Power Ratio of Transmissive Signal to Reflective Signal

Fig. 6(a) shows the sum rate versus the power ratio of transmissive signal to reflective signal ϵ with 100 IOS elements whose quantization bits is 3, i.e., M=100 and b=3.

The transmit power per AP P_{max} is set as 43 dBm. We assume that SUs are distributed in the area 5m from the IOS, and the ratio of transmissive SUs to all SUs is 0.5. It can be seen that as the power ratio of transmissive signal to reflective signal ϵ increases, the average rate of transmissive SUs grows and gradually converges to a stable value. In contrast, the average rate of reflective SUs decreases with a lower power ratio of transmissive signal to reflective signal and gradually flattens as ϵ continues to increase.

As shown in Fig. 6(b), we use the Jain's fairness index [42] to measure whether SUs are receiving a fair share of system resources with different power ratios of transmissive signal to reflective signal ϵ and different ratios of transmissive SUs to all SUs. Specifically, if all SUs are served fairy, the Jain's fairness index is 1. Otherwise, the Jain's fairness index tends to $\frac{1}{NK}$. We can observe that, as ϵ increases, a better fairness level can be achieved for the IOS aided system since the transmissive SUs can be better served. Moreover, it can be seen that the slope of the Jain's fairness index vs. ϵ grows with the ratio of transmissive SUs to all SUs.

 $^{^5\}mathrm{Due}$ to the wall which blocks the direct signal from AP n to its SUs in room n', the available rate of transmissive SUs is lower than that of reflective SUs.

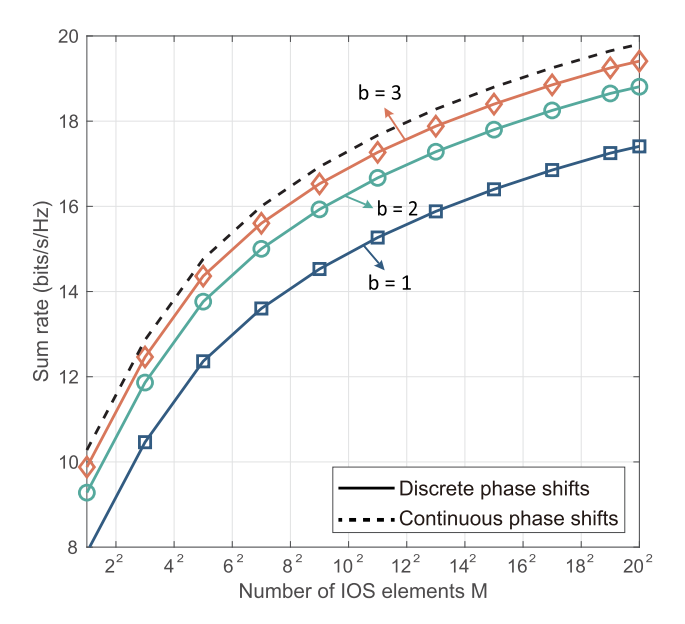


Fig. 8. Sum rate vs. the number of IOS elements ${\cal M}$ for different quantization bits b.

E. Impact of IOS Location

Fig. 7 shows the average data rate of the IOS aided system with different IOS locations where two APs are deployed at (0,25m) and (0,-25m), respectively. Namely, the value of each point illustrates the average data rate when the center of the IOS is located at (x, y). There are M = 100 IOS elements each of which works with b = 3 quantization bits for discrete phase shifts. The transmit power of each AP and the power ratio of transmissive signal to reflective signal ϵ are set as 43 dBm and 1, respectively. In Fig. 7(a), we can observe that, as the IOS gradually approaches to the AP n, SUs of AP n obtain a higher data rate since the path loss of reflective/transmissive links decrease. In contrast, as shown in Fig. 7(b), the average data rate of SUs of AP n' decreases when the distance between AP n' and the IOS increases. To achieve the tradeoff between the average data rate of these two APs, as shown in Fig. 7(c), the IOS should be located at the center of the room, i.e., (0,0), to maximize the data rate of all SUs.

F. Impact of Number of IOS Elements

Fig. 8 shows the impact of the number of IOS elements M on the sum rate performance with different quantization bits b and $P_{max}=43$ dBm. The distance between SUs and the IOS and the power ratio of transmissive signal to reflective signal ϵ are set as 5m and 1, respectively. We can observe that as the number of IOS elements increases, the sum rate grows rapidly with a small number of IOS elements and slows down as the number of IOS elements continues to increase. As b increases, the sum rate with discrete phase shifts gradually approaches that in the continuous case. The gap between the discrete and continuous cases is insignificant when $b \geq 3$, indicating that a small value of b is already enough to obtain a satisfactory performance.

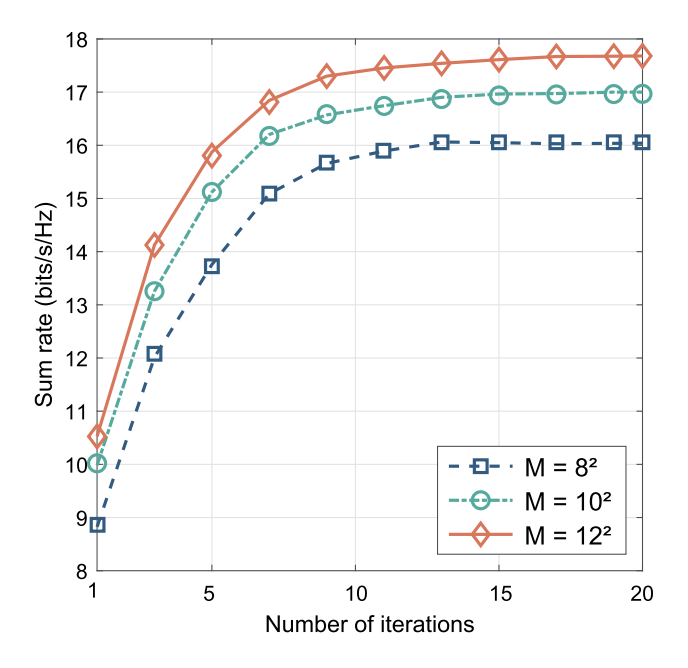


Fig. 9. Number of iterations to converge given different SUs.

G. Convergence

Fig. 9 shows the sum rate versus number of iterations for the different number of IOS elements. The transmit power per AP P_{max} is set as 43 dBm and the number of quantization bits for discrete phase shifts b is set as 3. The ratio of transmissive SUs to all SUs is set as 0.5. The distance between SUs and the IOS and the power ratio of transmissive signal to reflective signal ϵ are set as 5m and 1, respectively. It can be observed that the convergence speed slows down when the number of IOS elements M grows since more variables need to be optimized. We also observe that the algorithm can converge within 16 iterations for most cases. Therefore, the convergence analysis provided in Section IV-E is verified, and the complexity is low enough to be acceptable.

VI. CONCLUSION

In this paper, we have proposed an IOS aided system where an IOS is embedded in the wall between two APs to alleviate inter-cell interference. To maximize the sum rate, a hybrid beamforming scheme consisting of the digital beamforming at APs and IOS-based analog beamforming has been designed. Due to the distributed implementation of APs, we have performed the hybrid beamforming scheme in a distributed manner to mitigate inter-cell interference via IOS based analog beamforming design without any CSI exchange. Simulation results show the impact of the number of IOS elements, the number of quantization bits of discrete phase shifts, and the ratio of transmissive SUs on sum rate.

Three conclusion can be drawn from the numerical results, providing insights into the design of IOS aided systems.

 The IOS aided system based on a distributed hybrid beamforming design performs very close to the optimal centralized scheme, and has a better sum rate performance compared to existing ones including the

- conventional cellular system and two typical reflectingtype RIS aided systems.
- As the power ratio of transmissive signal to reflective signal increases, the average rate of transmissive/reflective SUs grows/decreases and gradually converges to a stable value, respectively, and a better fairness level can be achieved for the IOS aided communication.
- The average rate of all SUs decreases when the IOS gradually approaches to one AP, indicating that, in a two-room configuration, the IOS should be deployed at the center of the two rooms to achieve the maximum sum rate.

REFERENCES

- [1] D. Wang, Y. Zhang, H. Wei, X. You, X. Gao, and J. Wang, "An overview of transmission theory and techniques of large-scale antenna systems for 5G wireless communications," *Sci. China Inf. Sci.*, vol. 59, pp. 1–18, Aug. 2016.
- [2] T. Wang, S. Wang, and Z.-H. Zhou, "Machine learning for 5G and beyond: From model-based to data-driven mobile wireless networks," *China Commun.*, vol. 16, no. 1, pp. 165–175, Jan. 2019.
- [3] M. A. El Mossallamy, H. Zhang, L. Song, K. G. Seddik, Z. Han, and G. Y. Li, "Reconfigurable intelligent surfaces for wireless communications: Principles, challenges, and opportunities," *IEEE Trans. Cogn. Commun. Netw.*, vol. 6, no. 3, pp. 990–1002, Sep. 2020.
- [4] L. Subrt and P. Pechac, "Intelligent walls as autonomous parts of smart indoor environments," *IET Commun.*, vol. 6, no. 8, pp. 1004–1010, May 2012.
- [5] M. D. Renzo et al., "Smart radio environments empowered by reconfigurable AI meta-surfaces: An idea whose time has come," EURASIP J. Wireless Commun. Netw., vol. 2019, no. 1, pp. 1–20, May 2019.
- [6] J. Hu et al., "Reconfigurable intelligent surfaces based radio-frequency sensing: Design, optimization, and implementation," *IEEE J. Sel. Areas Commun.*, vol. 38, no. 11, pp. 2700–2716, Nov. 2020.
- [7] H. Zhang et al., "MetaRadar: Indoor localization by reconfigurable metamaterials," *IEEE Trans. Mobile Comput.*, early access, Dec. 14, 2020, doi: 10.1109/TMC.2020.3044603.
- [8] W. Tang et al., "MIMO transmission through reconfigurable intelligent surface: System design, analysis, and implementation," IEEE J. Sel. Areas Commun., vol. 38, no. 11, pp. 2683–2699, Nov. 2020.
- [9] H. Hashida, Y. Kawamoto, and N. Kato, "Intelligent reflecting surface placement optimization in air-ground communication networks toward 6G," *IEEE Wireless Commun.*, vol. 27, no. 6, pp. 146–151, Dec. 2020.
- [10] S. Zeng, H. Zhang, B. Di, Z. Han, and L. Song, "Reconfigurable intelligent surface (RIS) assisted wireless coverage extension: RIS orientation and location optimization," *IEEE Commun. Lett.*, vol. 25, no. 1, pp. 269–273, Jan. 2021.
- [11] C. Huang et al., "Holographic MIMO surfaces for 6G wireless networks: Opportunities, challenges, and trends," *IEEE Wireless Commun.*, vol. 27, no. 5, pp. 118–125, Oct. 2020.
- [12] S. Zeng et al., "Reconfigurable intelligent surfaces in 6G: Reflective, transmissive, or both?" IEEE Commun. Lett., vol. 25, no. 6, pp. 2063–2067, Jun. 2021.
- [13] S. Zhang, H. Zhang, B. Di, Y. Tan, Z. Han, and L. Song, "Beyond intelligent reflecting surfaces: Reflective-transmissive metasurface aided communications for full-dimensional coverage extension," *IEEE Trans.* Veh. Technol., vol. 69, no. 11, pp. 13905–13909, Nov. 2020.
- [14] G. Zhou, C. Pan, H. Ren, K. Wang, and A. Nallanathan, "Intelligent reflecting surface aided multigroup multicast miso communication systems," *IEEE Trans. Signal Process.*, vol. 68, pp. 3236–3251, 2020.
- [15] Y. Jia, C. Ye, and Y. Cui, "Analysis and optimization of an intelligent reflecting surface-assisted system with interference," in *Proc. IEEE Int. Conf. Commun. (ICC)*, Dublin, Ireland, Jun. 2020, pp. 8068–8082.
- [16] M. Fu, Y. Zhou, and Y. Shi, "Reconfigurable intelligent surface for interference alignment in MIMO device-to-device networks," in *Proc. IEEE Int. Conf. Commun. Workshops (ICC Workshops)*, Montreal, QC, Canada, Jun. 2021, pp. 1–6.
- [17] M. Elhattab, M.-A. Arfaoui, C. Assi, and A. Ghrayeb, "Reconfigurable intelligent surface assisted coordinated multipoint in downlink NOMA networks," *IEEE Commun. Lett.*, vol. 25, no. 2, pp. 632–636, Feb. 2021.

- [18] C. Pan et al., "Multicell MIMO communications relying on intelligent reflecting surfaces," *IEEE Trans. Wireless Commun.*, vol. 19, no. 8, pp. 5218–5233, Aug. 2020.
- [19] S. Huang, Y. Ye, M. Xiao, H. V. Poor, and M. Skoglund, "Decentralized beamforming design for intelligent reflecting surface-enhanced cell-free networks," *IEEE Wireless Commun. Lett.*, vol. 10, no. 3, pp. 673–677, Mar. 2021
- [20] Y. Zhang, B. Di, H. Zhang, J. Lin, Y. Li, and L. Song, "Reconfigurable intelligent surface aided cell-free MIMO communications," *IEEE Wireless Commun. Lett.*, vol. 10, no. 4, pp. 775–779, Apr. 2021.
- [21] Z. Zhang and L. Dai, "A joint precoding framework for wideband reconfigurable intelligent surface-aided cell-free network," *IEEE Trans. Signal Process.*, vol. 69, pp. 4085–4101, 2021.
- [22] H. L. Zhang, B. Y. Di, L. Y. Song, and Z. Han, "Reconfigurable intelligent surfaces assisted communications with limited phase shifts: How many phase shifts are enough?" *IEEE Trans. Veh. Technol.*, vol. 69, no. 4, pp. 4498–4502, Apr. 2020.
- [23] F. H. Danufane, M. D. Renzo, J. de Rosny, and S. Tretyakov, "On the path-loss of reconfigurable intelligent surfaces: An approach based on Green's theorem applied to vector fields," *IEEE Trans. Commun.*, vol. 69, no. 8, pp. 5573–5592, Aug. 2021.
- [24] F. Sohrabi and W. Yu, "Hybrid digital and analog beamforming design for large-scale antenna arrays," *IEEE J. Sel. Topics Signal Process.*, vol. 10, no. 3, pp. 501–513, Apr. 2016.
- [25] B. Di, H. Zhang, L. Song, Y. Li, Z. Han, and H. V. Poor, "Hybrid beamforming for reconfigurable intelligent surface based multi-user communications: Achievable rates with limited discrete phase shifts," *IEEE J. Sel. Areas Commun.*, vol. 38, no. 8, pp. 1809–1822, Aug. 2020.
- [26] J. Chen, Y.-C. Liang, H. V. Cheng, and W. Yu, "Channel estimation for reconfigurable intelligent surface aided multi-user MIMO systems," 2019, arXiv:1912.03619.
- [27] D. Mishra and H. Johansson, "Channel estimation and low-complexity beamforming design for passive intelligent surface assisted MISO wireless energy transfer," in *Proc. IEEE Int. Conf. Acoust., Speech Signal Process. (ICASSP)*, Brighton, U.K., May 2019, pp. 4659–4663.
- [28] H. Liu, X. Yuan, and Y.-J.-A. Zhang, "Matrix-calibration-based cascaded channel estimation for reconfigurable intelligent surface assisted multiuser MIMO," *IEEE J. Sel. Areas Commun.*, vol. 38, no. 11, pp. 2621–2636, Nov. 2020.
- [29] S. Zhang et al., "Intelligent omni-surfaces: Ubiquitous wireless transmission by reflective-refractive metasurfaces," IEEE Trans. Wireless Commun., vol. 21, no. 1, pp. 219–233, Jan. 2022.
- [30] H. Zhang et al., "Intelligent omni-surfaces for full-dimensional wireless communications: Principles, technology, and implementation," IEEE Commun. Mag., vol. 60, no. 2, pp. 39–45, Feb. 2022.
- [31] C. Pfeiffer and A. Grbic, "Metamaterial Huygens' surfaces: Tailoring wave fronts with reflectionless sheets," *Phys. Rev. Lett.*, vol. 110, no. 19, pp. 1–5, May 2013.
- [32] E. Björnson and L. Sanguinetti, "Rayleigh fading modeling and channel hardening for reconfigurable intelligent surfaces," *IEEE Wireless Commun. Lett.*, vol. 10, no. 4, pp. 830–834, Apr. 2021.
- [33] X. Yu, J.-C. Shen, J. Zhang, and K. B. Letaief, "Alternating minimization algorithms for hybrid precoding in millimeter wave MIMO systems," *IEEE J. Sel. Topics Signal Process.*, vol. 10, no. 3, pp. 485–500, May 2016.
- [34] Y. Ye, M. Xiao, and M. Skoglund, "Mobility-aware content preference learning in decentralized caching networks," *IEEE Trans. Cognit. Commun. Netw.*, vol. 6, no. 1, pp. 62–73, Mar. 2020.
- [35] Y. Ye, H. Chen, Z. Ma, and M. Xiao, "Decentralized consensus optimization based on parallel random walk," *IEEE Commun. Lett.*, vol. 24, no. 2, pp. 391–395, Feb. 2020.
- [36] K. Shen and W. Yu, "Fractional programming for communication systems—Part II: Uplink scheduling via matching," *IEEE Trans. Signal Process.*, vol. 66, no. 10, pp. 2631–2644, May 2018.
- [37] K. Shen, W. Yu, L. Zhao, and D. P. Palomar, "Optimization of MIMO device-to-device networks via matrix fractional programming: A minorization-maximization approach," *IEEE/ACM Trans. Netw.*, vol. 27, no. 5, pp. 2164–2177, Oct. 2019.
- [38] K. Shen and W. Yu, "Fractional programming for communication systems—Part I: Power control and beamforming," *IEEE Trans. Signal Process.*, vol. 66, no. 10, pp. 2616–2630, May 2018.
- [39] L. Wu, P. Babu, and D. P. Palomar, "Transmit waveform/receive filter design for MIMO radar with multiple waveform constraints," *IEEE Trans. Signal Process.*, vol. 66, no. 6, pp. 1526–1540, May 2018.

- [40] C. Huang, A. Zappone, G. C. Alexandropoulos, M. Debbah, and C. Yuen, "Reconfigurable intelligent surfaces for energy efficiency in wireless communication," *IEEE Trans. Wireless Commun.*, vol. 18, no. 8, pp. 4157–4170, Aug. 2019.
- [41] M. Series, "Guidelines for evaluation of radio interface technologies for IMT-Advanced," ITU, Geneva, Switzerland, Tech. Rep. ITU-R M.2135-1, Dec. 2009.
- [42] R. Jain, D.-M. Chiu, and W. R. Hawe, "A quantitative measure of fairness and discrimination for resource allocation in shared computer system," DEC Res., Hudson, MA, USA, Tech. Rep. TR-301, Sep. 1984, vol. 38.



Yutong Zhang (Graduate Student Member, IEEE) received the B.S. degree in electronics information science and technology from Yunnan University, Kunming, China, in 2017, and the M.E. degree from the School of Software and Microelectronics, Peking University, China, in 2020. She is currently pursuing the Ph.D. degree with the Department of Electronics, Peking University, Beijing, China. Her current research interests include intelligent surface, wireless communications, and edge computing.



Zhu Han (Fellow, IEEE) received the B.S. degree in electronic engineering from Tsinghua University, Beijing, China, in 1997, and the M.S. and Ph.D. degrees in electrical and computer engineering from the University of Maryland, College Park, MD, USA, in 1999 and 2003, respectively. From 2000 to 2002, he was a Research and Development Engineer at JDSU, Germantown, MD, USA. From 2003 to 2006, he was a Research Associate at the University of Maryland. From 2006 to 2008, he was an Assistant Professor at Boise State Uni-

versity, Boise, ID, USA. He is currently a John and Rebecca Moores Professor at the Electrical and Computer Engineering Department and the Computer Science Department, University of Houston, Houston, TX, USA. His research interests include wireless resource allocation and management, wireless communications and networking, game theory, big data analysis, security, and smart grid. He received an NSF Career Award in 2010, the Fred W. Ellersick Prize of the IEEE Communication Society in 2011, the EURASIP Best Paper Award for the Journal on Advances in Signal Processing in 2015, the IEEE Leonard G. Abraham Prize in the field of Communications Systems (Best Paper Award in IEEE JSAC) in 2016, and several best paper awards in IEEE conferences. He is also the winner of the 2021 IEEE Kiyo Tomiyasu Award for outstanding early to mid-career contributions to technologies holding the promise of innovative applications, with the following citation: for contributions to game theory and distributed management of autonomous communication networks. He is 1% highly cited researcher since 2017 according to Web of Science. He was an IEEE Communications Society Distinguished Lecturer from 2015 to 2018, an AAAS fellow since 2019, and an ACM Distinguished Member since 2019.



Boya Di (Member, IEEE) received the B.S. and Ph.D. degrees in electronic engineering from the Department of Electronics, Peking University, Beijing, China, in 2014 and 2019, respectively. She was a Post-Doctoral Researcher at Imperial College London. She is currently an Assistant Professor at Peking University. Her current research interests include reconfigurable intelligent surfaces, multiagent systems, edge computing, vehicular networks, and aerial access networks. She received the Best Doctoral Thesis Award from the China Education

Society of Electronics in 2019. She was also a recipient of 2021 IEEE ComSoc Asia-Pacific Outstanding Paper Award. She has been serving as an Associate Editor for IEEE TRANSACTIONS ON VEHICULAR TECHNOLOGY since June 2020. She has also served as a Workshop Co-Chair for IEEE WCNC 2020 and 2021.



H. Vincent Poor (Life Fellow, IEEE) received the Ph.D. degree in EECS from Princeton University in 1977. From 1977 to 1990, he was on the faculty of the University of Illinois at Urbana–Champaign, Champaign, IL, USA. Since 1990, he has been on the faculty at Princeton University, where he is currently the Michael Henry Strater University Professor. From 2006 to 2016, he served as the Dean of Princeton's School of Engineering and Applied Science. He has also held visiting appointments at several other universities, including most recently at

Berkeley and Cambridge. His research interests include information theory, machine learning, and network science, and their applications in wireless networks, energy systems, and related fields. Among his publications in these areas is the forthcoming book *Machine Learning and Wireless Communications* (Cambridge University Press). He is a member of the National Academy of Engineering and the National Academy of Sciences and a Foreign Member of the Chinese Academy of Sciences, the Royal Society, and other national and international academies. He received the IEEE Alexander Graham Bell Medal in 2017.



Hongliang Zhang (Member, IEEE) received the B.S. and Ph.D. degrees from the School of Electrical Engineering and Computer Science, Peking University, in 2014 and 2019, respectively. He was a Post-Doctoral Fellow with the Electrical and Computer Engineering Department, University of Houston, Houston, TX, USA. He is currently a Post-Doctoral Associate with the Department of Electrical and Computer Engineering, Princeton University, Princeton, NJ, USA. His current research interests include reconfigurable intelligent surfaces, aerial access net-

works, optimization theory, and game theory. He has served as a TPC Member for many IEEE conferences, such as Globecom, ICC, and WCNC. He received the Best Doctoral Thesis Award from the Chinese Institute of Electronics in 2019. He was also a recipient of the 2021 IEEE Comsoc Heinrich Hertz Award for Best Communications Letters and the 2021 IEEE ComSoc Asia-Pacific Outstanding Paper Award. He is currently an Editor of IEEE COMMUNICATIONS LETTERS, IET Communications, and Frontiers in Signal Processing. He is an Exemplary Reviewer of IEEE TRANSACTIONS ON COMMUNICATIONS in 2020. He has served as a Guest Editor for several journals, such as IEEE Internet of Things Journal and Journal of Communications and Networks.



Lingyang Song (Fellow, IEEE) received the Ph.D. degree from the University of York, York, U.K., in 2007. He worked as a Research Fellow at the University of Oslo, Oslo, Norway, until rejoining Philips Research, U.K., in March 2008. In May 2009, he joined the Department of Electronics, School of Electronics Engineering and Computer Science, Peking University, where he is currently a Boya Distinguished Professor. His main research interests include wireless communication and networks, signal processing, and machine learning.

He received the K. M. Stott Prize for Excellent Research from the University of York. He was also a recipient of the IEEE Leonard G. Abraham Prize in 2016 and the IEEE Asia Pacific (AP) Young Researcher Award in 2012. He has been an IEEE Distinguished Lecturer since 2015.